

Nonlinear Bandwidth and Bode Diagrams based on Scaled Relative Graphs

Julius P.J. Krebbekx¹, Roland Tóth^{1,2}, Amritam Das¹

Abstract—Scaled Relative Graphs (SRGs) provide a novel graphical frequency domain method for the analysis of nonlinear systems. In this paper, we use the restriction of the SRG to particular input spaces to compute frequency-dependent gain bounds for incrementally stable nonlinear systems. This leads to a nonlinear (NL) generalization of the Bode diagram, where the sinusoidal, harmonic, and subharmonic inputs are considered separately. When applied to the analysis of the NL loop transfer and sensitivity, we define a notion of bandwidth for both the open-loop and closed-loop, compatible with the LTI definitions. We illustrate the power of our method on the analysis of a DC motor with a parasitic nonlinearity, verifying our results in simulations.

I. INTRODUCTION

In the case of Linear Time Invariant (LTI) systems, graphical analysis using the Nyquist diagram [1] and the Bode diagram [2] is the cornerstone of control engineering. They are easy to use and allow for intuitive analysis and controller design methods. However, it is unclear how to generalize graphical frequency domain methods to nonlinear system analysis and controller design.

When pushing the performance of dynamical systems through control design, the Nonlinear (NL) dynamics start to play a crucial role. Inspired by the success of analyzing performance through Bode diagrams in the LTI case, e.g. for mixed sensitivity shaping [3], there have been multiple attempts to generalize the Bode diagram to the NL case. The describing function [4], which is approximative, has been the first step in this direction, successfully applied in applications [4]–[6]. Most modern and non-approximative methods focus on sinusoidal inputs [6], [7], but other works also consider higher-order harmonics in the input [8] or specific periodic inputs [9].

The Scaled Relative Graph (SRG) [10] proposed in [11] is a new graphical method to analyze nonlinear feedback systems. It is an exact method, and it is intuitive because of its close connection to the Nyquist diagram. Moreover, SRG analysis can provide performance bounds in terms of (incremental) L_2 -gain. Originally, it was applicable for Single-Input-Single-Output (SISO) systems only and has been recently extended to include unstable elements in the loop [12]. While practical stability analysis is an important outcome of the SRG framework, our aim is to take one step further and establish a frequency domain performance shaping tool for NL systems.

Hence, in this paper, we develop novel non-approximative frequency domain tools for Time Invariant (TI) incrementally stable NL systems by leveraging the SRG framework. Compared to [13], incremental stability replaces the assumption of a convergent system. The central idea is to compute the incremental gain for an input space of signals with a common period, where the SRG is the central computational tool. By evaluating these gains over a grid of frequencies, one obtains a Bode diagram for the NL system. The NL Bode diagram is used to define the NL bandwidth for the loop transfer and sensitivity, compatible with the LTI definition.

Our method can reproduce most aspects of existing work, such as sinusoidal input Bode diagrams. Also, our results are more general since we are able to compute the gain for any frequency and *arbitrary* higher harmonics, but amplitude-dependent results, compared to, e.g. [13], are not yet reflected in our approach. An entirely novel aspect of our work is the gain for signals with *subharmonics*, which allows low-frequency analysis of sensitivity functions, going beyond sinusoidal inputs. Finally, all our computations are based on modular interconnections of LTI and NL operators, instead of relying on state-space realizations, making the application of our method more accessible to engineers.

This paper is structured as follows. In Section II, we present the required preliminaries. In Section III, we derive a method to analyze incrementally stable systems in the frequency domain, leading to our definition of the NL Bode plot. We show how SRGs are used to compute the NL Bode diagrams in Section IV, focusing on the loop transfer and the sensitivity. Finally, we apply our results to a practical design example in Section V and present our conclusions in Section VI.

II. PRELIMINARIES

A. Notation and Conventions

Let \mathbb{R} and \mathbb{C} denote the field real and complex numbers, respectively, with $\mathbb{R}_{>0} = (0, \infty)$, $\mathbb{R}_{\geq 0} = [0, \infty)$ and $\mathbb{C}_{\text{Re}>0} = \{a + jb \mid a \in \mathbb{R}_{>0}, b \in \mathbb{R}\}$, where j is the imaginary unit. We denote the complex conjugate of $z = a + jb \in \mathbb{C}$ as $\bar{z} = a - jb$. Let \mathcal{L} denote a Hilbert space, with inner product $\langle \cdot | \cdot \rangle_{\mathcal{L}} : \mathcal{L} \times \mathcal{L} \rightarrow \mathbb{C}$ and norm $\|x\|_{\mathcal{L}} := \sqrt{\langle x | x \rangle_{\mathcal{L}}}$. For sets $A, B \subset \mathbb{C}$, the sum and product sets are defined as $A + B := \{a + b \mid a \in A, b \in B\}$ and $AB := \{ab \mid a \in A, b \in B\}$, respectively. A disk in the complex plane is $D_r(x) = \{z \in \mathbb{C} \mid |z - x| \leq r\}$. Denote $D_{[\alpha, \beta]}$ the disk in \mathbb{C} centered on \mathbb{R} which intersects \mathbb{R} in $[\alpha, \beta]$. The radius of a set $\mathcal{C} \subset \mathbb{C}$ is defined by $r_{\min}(\mathcal{C}) := \min_{r>0} : \mathcal{C} \subset D_r(0)$.

¹Control Systems group, Department of Electrical Engineering, Eindhoven University of Technology, The Netherlands.

²Systems and Control Lab, HUN-REN Institute for Computer Science and Control, Budapest, Hungary. E-mail: {j.p.j.krebbekx, r.toth, am.das}@tue.nl

B. Signals, Systems and Stability

Denote a field $\mathbb{F} \in \{\mathbb{R}^n, \mathbb{C}^n\}$, where $n = 1$ is assumed, unless otherwise specified, since this work focuses on SISO continuous-time systems. A Hilbert space of particular interest is $L_2(\mathbb{T}, \mathbb{F}) := \{f : \mathbb{T} \rightarrow \mathbb{F} \mid \|f\|_2 < \infty\}$, where the norm is induced by the inner product $\langle f|g \rangle := \int_{\mathbb{T}} \bar{f}(t)g(t)dt$, and \bar{f} denotes the complex conjugate, and $\mathbb{T} \in \{\mathbb{R}_{\geq 0}, [0, T]\}$ for any $T > 0$ is the domain. For brevity, we denote $L_2(\mathbb{R}_{\geq 0}, \mathbb{F})$ as $L_2(\mathbb{F})$, $L_2(\mathbb{R}_{\geq 0}, \mathbb{R})$ as L_2 and, if the time domain is finite, $L_2([0, T], \mathbb{R})$ as $L_2([0, T])$.

For any $T \in \mathbb{R}_{\geq 0}$, define the truncation operator $P_T : L_2(\mathbb{F}) \rightarrow L_2(\mathbb{F})$ as

$$(P_T u)(t) := \begin{cases} u(t) & t \leq T, \\ 0 & t > T. \end{cases} \quad (1)$$

The extension of $L_2(\mathbb{F})$, see Ref. [14], is defined as

$$L_{2e}(\mathbb{F}) := \{u : \mathbb{R}_{\geq 0} \rightarrow \mathbb{F} \mid \|P_T u\|_2 < \infty \text{ for all } T \in \mathbb{R}_{\geq 0}\}.$$

The space $L_{2e}(\mathbb{R})$, which we denote from now on as L_{2e} , will be the most frequently used space of signals. Note that the extension is particularly useful since it includes periodic signals, which are otherwise excluded from L_2 .

Periodic signals $v \in L_{2e}$ can also be viewed as elements in $L_2([0, T])$, where T is the period of the signal, i.e. $v(t) = v(t+T)$ for all $t \in [0, \infty)$. Any $u \in L_2([0, T])$ can be written in Fourier series as

$$u(t) = \sum_{k \in \mathbb{Z}} \hat{u}_k e^{2\pi jkt/T}, \quad (2)$$

where $\hat{u}_k \in \mathbb{C}$ are the Fourier coefficients. One can define the Root-Mean-Square (RMS) norm of the signal as $\|u\|_{\text{RMS}} = \sqrt{\sum_{k \in \mathbb{Z}} |\hat{u}_k|^2}$, which relates to the L_2 -norm as $\|u\|_{L_2([0, T])} = \sqrt{T} \|u\|_{\text{RMS}}$.

Systems are modeled as operators $R : L_{2e} \rightarrow L_{2e}$. A system is said to be causal if it satisfies $P_T(Ru) = P_T(R(P_T u))$, i.e., the output at time t is independent of the signal at times greater than t . Unless specified otherwise, we will always assume causality.

Given an operator R on a L_2 , the induced incremental norm of the operator is defined (similar to the notation in [15]) as

$$\Gamma(R) := \sup_{u_1, u_2 \in L_2} \frac{\|Ru_1 - Ru_2\|_2}{\|u_1 - u_2\|_2}. \quad (3)$$

The radius of the SRG corresponds to the incremental induced gain as $r_{\min}(\text{SRG}(R)) = \Gamma(R)$ in terms of Eqs. (3).

For causal systems, the induced incremental operator norm on L_2 carries over to L_{2e} since $\|P_T(R(P_T u))\|_2 \leq \|R(P_T u)\|_2$ and $P_T u \in L_2$ for all $u \in L_{2e}$ where P_T is defined in (1). We define the incremental L_2 -gain of a causal operator $R : L_{2e}(\mathbb{F}) \rightarrow L_{2e}(\mathbb{F})$ as $\Gamma(R)$, i.e., the induced incremental operator norm from Eq. (3). A causal system R is said to be incrementally L_2 -stable if $\Gamma(R) < \infty$. A system R is called L_2 -stable if $\|u\|_2 < \infty$ implies $\|Ru\|_2 < \infty$. If $R(0) = 0$ holds, then an incremental L_2 -stability implies L_2 -stability.

C. Complex Geometry

We denote the line segment between $z_1, z_2 \in \mathbb{C}$ as $[z_1, z_2] := \{\alpha z_1 + (1 - \alpha)z_2 \mid \alpha \in [0, 1]\}$. Let the right-hand arc, denoted by $\text{Arc}^+(z, \bar{z})$, be the circle segment of the circle that is centered at the origin and intersects z, \bar{z} , with real part greater than $\text{Re } z$. The left-hand arc, denoted $\text{Arc}^-(z, \bar{z})$, is similarly defined, but with real part smaller than $\text{Re } z$.

Let $z_1, z_2 \in \mathbb{C}_{\text{Im} \geq 0}$ where we assume w.l.o.g. that $\text{Re } z_1 \leq \text{Re } z_2$. Denote $\text{Circ}(z_1, z_2)$ the unique circle through z_1, z_2 centered on \mathbb{R} . Let

$$\text{Arc}_{\min}(z_1, z_2) = \{z \in \text{Circ}(z_1, z_2) \mid \text{Re } z_1 \leq \text{Re } z \leq \text{Re } z_2, \text{Im } z \geq 0\}.$$

Definition 1 (h-convex). *A set $S \subset \mathbb{C}_{\text{Im} \geq 0}$ is h-convex if*

$$z_1, z_2 \in S \iff \text{Arc}_{\min}(z_1, z_2) \subset S.$$

Given a set of points $P \subset \mathbb{C}_{\text{Im} \geq 0}$, the h-convex hull of P is the smallest set $\bar{P} \supset P$ that is h-convex. We denote the h-convex hull as $\bar{P} = \text{co}_{\text{Be-KI}}(P)$.

For a set $P \in \mathbb{C}$ that is equal to its complex conjugate $\bar{P} = P$, i.e., is symmetric w.r.t. the real axis, h-convexity can be studied for $P_+ := P \cap \mathbb{C}_{\text{Im} \geq 0}$. In that case, the h-convex hull is defined $\text{co}_{\text{Be-KI}}(P) = \text{co}_{\text{Be-KI}}(P_+) \cup \overline{\text{co}_{\text{Be-KI}}(P_+)}$.

D. Scaled Relative Graphs

We now turn to the definition and properties of the Scaled Relative Graph (SRG) as introduced by Ryu et al. in [10]. We follow closely the exposition of the SRG as given by Chaffey et al. in [11].

1) *Definitions:* Let \mathcal{L} be a Hilbert space, and $R : \mathcal{L} \rightarrow \mathcal{L}$ an operator. The angle between $u, y \in \mathcal{L}$ is defined as

$$\angle(u, y) := \cos^{-1} \frac{\text{Re} \langle u|y \rangle}{\|u\| \|y\|} \in [0, \pi]. \quad (4)$$

Given $u_1, u_2 \in \mathcal{U} \subset \mathcal{L}$, we define the set of complex numbers

$$z_R(u_1, u_2) := \left\{ \frac{\|Ru_1 - Ru_2\|}{\|u_1 - u_2\|} e^{\pm j\angle(u_1 - u_2, Ru_1 - Ru_2)} \right\}.$$

The SRG of R over the set \mathcal{U} is defined as

$$\text{SRG}_{\mathcal{U}}(R) := \bigcup_{u_1, u_2 \in \mathcal{U}} z_R(u_1, u_2). \quad (5)$$

If $\mathcal{U} = \mathcal{L}$, we simply write $\text{SRG}(R)$.

2) *Operations on SRGs:* The facts presented here are proven in [10, Chapter 4].

Inversion of a point $z = re^{j\omega} \in \mathbb{C}$ is defined as the Möbius inversion $re^{j\omega} \mapsto (1/r)e^{j\omega}$. An operator R satisfies the *chord property* if, for all $z \in \text{SRG}(R) \setminus \{\infty\}$, it holds that $[z, \bar{z}] \subset \text{SRG}(R)$. An operator R is said to satisfy the left-hand (right-hand) arc property if for all $z \in \text{SRG}(R)$, it holds that $\text{Arc}^-(z, \bar{z}) \subset \text{SRG}(R)$ ($\text{Arc}^+(z, \bar{z}) \subset \text{SRG}(R)$). If R satisfies the left-hand, right-hand, or both arc properties, it is said to satisfy an arc property.

Proposition 1. *Let $0 \neq \alpha \in \mathbb{R}$ and let R, S be arbitrary operators on the Hilbert space \mathcal{L} . Then,*

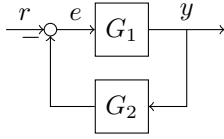


Fig. 1: Block diagram of a general feedback interconnection where G_1 and G_2 can be LTI or NL static or dynamic blocks.

- $\text{SRG}(\alpha R) = \text{SRG}(R\alpha) = \alpha \text{SRG}(R)$,
- $\text{SRG}(I+R) = 1 + \text{SRG}(R)$, where I denotes the identity on \mathcal{L} ,
- $\text{SRG}(R^{-1}) = (\text{SRG}(R))^{-1}$.
- If at least one of R, S satisfies the chord property, then $\text{SRG}(R+S) \subset \text{SRG}(R) + \text{SRG}(S)$.
- If at least one of R, S satisfies an arc property, then $\text{SRG}(RS) \subset \text{SRG}(R)\text{SRG}(S)$.

If the SRGs above contain ∞ or are the empty set, the above operations are slightly different, see [10].

3) *Stability analysis*: SRGs are the tool to compute the incremental L_2 -gain of a system. We cite the central result from [11], which considers any system G_1 in feedback with another system G_2 , as displayed in Fig. 1.

Proposition 2. Consider G_1, G_2 be operators on L_{2e} , where $\Gamma(G_1) < \infty$ and G_2 satisfies for all $\tau \in (0, 1]$

$$\text{SRG}(G_1)^{-1} \cap -\tau \text{SRG}(G_2) = \emptyset,$$

and at least one of G_1, G_2 obeys the chord property. Then, the feedback connection in Fig. 1 has an incremental L_2 -gain bound of $1/r_m$, where the minimal distance between $\text{SRG}(G_1)^{-1}$ and $-\text{SRG}(G_2)$ is denoted as r_m .

Note that Proposition 2 works only in the case of stable open-loop plants G_1 . In [12], Proposition 2 has been extended to the case where G_1 is now an unstable LTI operator.

III. FREQUENCY DOMAIN ANALYSIS OF INCREMENTALLY STABLE SYSTEMS

To formulate an effective frequency-domain interpretation of NL systems, the core idea of this work is to exploit the properties of incrementally stable time-invariant (TI) systems. The most important property is the fact that, for such NL systems, periodic inputs are mapped to outputs of the same frequency.

Suppose that $R : L_{2e} \rightarrow L_{2e}$ is causal and has finite incremental gain $\Gamma(R)$. We call R TI if for all $u \in L_{2e}$, it is true that $\sigma_T(Ru)(t) = (R\sigma_T(u))(t)$ for all $T \geq 0$, where the backward time shift operator $\sigma_T : L_{2e} \rightarrow L_{2e}$ is defined as

$$(\sigma_T f)(t) = \begin{cases} 0 & \text{if } 0 \leq t < T, \\ f(t-T) & \text{if } t \geq T. \end{cases}$$

The reason for using *backward* TI is that the operator acts on signals starting at $t = 0$, which hinders the usual TI definition $\sigma_T(Ru)(t) = (R\sigma_T(u))(t)$ for all $T \in \mathbb{R}$.

A. The Period Preserving Property

Let u be a signal with period T and $v = \sigma_T u$. Note that $u(t) = v(t)$ for $t \geq T$. Using incremental stability, we have

$$\|Ru - \sigma_T Ru\|_2 \leq \Gamma(R) \|u - v\|_2 = \Gamma(R) \|P_T u\|_2,$$

which is finite while $\lim_{\tau \rightarrow \infty} \|P_\tau(Ru)\|_2 = \infty$. Using this result, one can conclude that

$$(Ru)(t) - (Ru)(t-T) \xrightarrow{t \rightarrow \infty} 0. \quad (6)$$

In other words, when given an input with period T , the output $y = Ru$ converges to a signal \tilde{y} with period T as well.

Now we can write the input u and output limit \tilde{y} as Fourier series with finite RMS norms. Using Eq. (6), we derive the following lemma, but omit the proof for the sake of brevity.

Lemma 1. For any pair $u_1, u_2 \in L_{2e}$ with the same period

$$\frac{\|Ru_1 - Ru_2\|_2}{\|u_1 - u_2\|_2} = \frac{\|\tilde{y}_1 - \tilde{y}_2\|_{\text{RMS}}}{\|u_1 - u_2\|_{\text{RMS}}},$$

and consequently

$$\Gamma(R) = \sup_{u_1, u_2} \frac{\|\tilde{y}_1 - \tilde{y}_2\|_{\text{RMS}}}{\|u_1 - u_2\|_{\text{RMS}}}, \quad (7)$$

allowing to interpret the incremental gain as the RMS gain.

This lemma serves as the cornerstone of our frequency domain analysis of NL systems. Note that Eq. (7) is equivalent to the \mathcal{H}_∞ -norm if R is an LTI operator (see [16, Ch. 4]).

B. Nonlinear Bode Plots

We can now exploit the fact that incrementally stable systems preserve the period of the input. When an input has period T , we call $\omega = 2\pi/T$ the *base harmonic*. The key idea is now to compute the gain Eq. (7) for a specific space of input signals that corresponds to a given base harmonic.

Definition 2. For a frequency $\omega \in \mathbb{R}_{>0}$, we define

$$\mathcal{U}_\omega := \{u \in L_{2e} \mid u(t) = a \sin(\omega t + \phi), \quad a, \phi \in \mathbb{R}\}, \quad (8a)$$

$$\overline{\mathcal{U}}_\omega := \{u \in L_{2e} \mid u(t) = \sum_{n \in \mathbb{Z}} \hat{u}_n e^{j\omega n t}\}, \quad (8b)$$

$$\underline{\mathcal{U}}_\omega := \{u \in L_{2e} \mid u(t) = \sum_{0 \neq n \in \mathbb{Z}} \hat{u}_n e^{j(\omega/n)t}\}, \quad (8c)$$

which are called the *sinusoidal, harmonic and subharmonic input spaces, respectively*. The input space specific gains are defined as

$$\Gamma_\omega(R) = \sup_{u_1, u_2 \in \mathcal{U}_\omega} \frac{\|\tilde{y}_1 - \tilde{y}_2\|_{\text{RMS}}}{\|u_1 - u_2\|_{\text{RMS}}}, \quad (9a)$$

$$\overline{\Gamma}_\omega(R) = \sup_{u_1, u_2 \in \overline{\mathcal{U}}_\omega} \frac{\|\tilde{y}_1 - \tilde{y}_2\|_{\text{RMS}}}{\|u_1 - u_2\|_{\text{RMS}}}, \quad (9b)$$

$$\underline{\Gamma}_\omega(R) = \sup_{u_1, u_2 \in \underline{\mathcal{U}}_\omega} \frac{\|\tilde{y}_1 - \tilde{y}_2\|_{\text{RMS}}}{\|u_1 - u_2\|_{\text{RMS}}}. \quad (9c)$$

Note that since $\mathcal{U}_\omega \subset \overline{\mathcal{U}}_\omega \subset L_{2e}$ and $\mathcal{U}_\omega \subset \underline{\mathcal{U}}_\omega \subset L_{2e}$ for all $\omega \in [0, \infty)$, it holds that

$$\Gamma_\omega(R) \leq \overline{\Gamma}_\omega(R) \leq \Gamma(R), \quad \Gamma_\omega(R) \leq \underline{\Gamma}_\omega(R) \leq \Gamma(R). \quad (10)$$

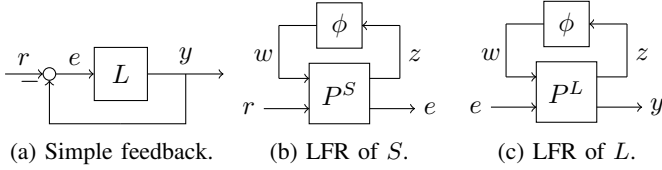


Fig. 2: Interconnections for the analysis of simple feedback.

Moreover, because $\lim_{\omega \rightarrow \infty} \underline{\mathcal{U}}_\omega = \lim_{\omega \downarrow 0} \overline{\mathcal{U}}_\omega = L_{2e}$, we can conclude that

$$\lim_{\omega \rightarrow \infty} \underline{\Gamma}_\omega(R) = \lim_{\omega \downarrow 0} \overline{\Gamma}_\omega(R) = \Gamma(R). \quad (11)$$

The *NL Bode plot* is obtained by plotting Eqs. (9a), (9b) and (9c) as function of $\omega \in \mathbb{R}_{>0}$ in one graph, analogously to a conventional Bode plot. To the best knowledge of the authors, the *NL Bode plot* provides a novel way to study the frequency domain behavior of nonlinear operators, under the assumption that the operator is causal and incrementally stable. We will compare our result to existing methods in Section IV-E.

IV. NONLINEAR BODE DIAGRAMS USING SCALED RELATIVE GRAPHS

A. The Feedback Interconnection for Loop Shaping

Analogously to the Nyquist criterion, we are interested in the simple feedback interconnection as shown in Fig. 2a, where $L : L_{2e} \rightarrow L_{2e}$ is the loop transfer $y = Le$. For loop shaping, we consider both the loop transfer, as well as the sensitivity $e = Sr$ given by $S = (1 + L)^{-1}$. To simplify the analysis, we focus on SISO systems with only one nonlinearity ϕ in the interconnection. This allows us to write both L and S in a Linear Fractional Representation (LFR) form using $w = \phi(z)$ and

$$\begin{pmatrix} z \\ y \end{pmatrix} = \underbrace{\begin{pmatrix} P_{zw}^L & P_{ze}^L \\ P_{yw}^L & P_{ye}^L \end{pmatrix}}_{=: PL} \begin{pmatrix} w \\ e \end{pmatrix}, \quad \begin{pmatrix} z \\ e \end{pmatrix} = \underbrace{\begin{pmatrix} P_{zw}^S & P_{zr}^S \\ P_{ew}^S & P_{er}^S \end{pmatrix}}_{=: PS} \begin{pmatrix} w \\ r \end{pmatrix},$$

as depicted in Figs. 2c and 2b, respectively, which results in the operators

$$L = P_{yw}^L (\phi^{-1} - P_{zw}^L)^{-1} P_{ze}^L + P_{ye}^L, \quad (12)$$

$$S = P_{ew}^S (\phi^{-1} - P_{zw}^S)^{-1} P_{zr}^S + P_{er}^S, \quad (13)$$

where all operators P are SISO and LTI, and $P_{yw}^L, P_{ze}^L, P_{ye}^L, P_{zw}^S, P_{zr}^S, P_{er}^S$ are assumed to be stable. The stability of both operators L, S depends only on $(\phi^{-1} - P_{zw}^\bullet)^{-1}$, where $\bullet \in \{S, L\}$, which can be analyzed using Proposition 2 by picking $G_1 = \phi, G_2 = -P_{zw}^\bullet$. If P_{zw}^\bullet is unstable, one must use the SRG method for unstable systems from [12]. Stability of these loops must hold for our method to work.

B. Nonlinear Bandwidth

Now that we have a definition of the NL Bode diagram, in terms of Eq. (9), we can also define a *bandwidth* (BW) for the NL loop transfer L and sensitivity S . The following two definitions are entirely analogous to the LTI case [3].

Definition 3. The closed-loop bandwidth is the smallest value ω_B such that $|\underline{\Gamma}_{\omega_B}(S)|$ crosses $1/\sqrt{2}$ from below.

Definition 4. The open-loop bandwidth is the smallest value ω_c such that $|\overline{\Gamma}_{\omega_c}(L)|$ crosses 1 from above.

We will show later through an example why these definitions make sense and what practical use they represent.

C. Frequency Domain Analysis

SRG analysis can be directly used for computing the norms in Eq. (9) for the sensitivity S and loop transfer L . More precisely, one can use the SRG restricted to a specific input space $\text{SRG}_{\mathcal{U}}(S), \text{SRG}_{\mathcal{U}}(L)$ in Eq. (5), where now the input space is $\mathcal{U} \in \{\underline{\mathcal{U}}_\omega, \overline{\mathcal{U}}_\omega, \underline{\mathcal{U}}_\omega\}$, as defined in Eq. (8). For the remainder of this section, we focus on S , since the analysis is identical for L .

1) *The SRG of an LTI operator for a specific input space:* The first step is to consider to what input spaces different operators map to. LTI operators map each of the spaces $\mathcal{U} \in \{\underline{\mathcal{U}}_\omega, \overline{\mathcal{U}}_\omega, \underline{\mathcal{U}}_\omega\}$ to itself. Because of this property, one can determine the SRG of an LTI operator $G(s)$ for a specific input space:

$$\text{SRG}_{\underline{\mathcal{U}}_\omega}(G) = \{G(\pm j\omega)\}, \quad (14a)$$

$$\text{SRG}_{\overline{\mathcal{U}}_\omega}(G) = \text{co}_{\text{Be-KI}}(\{G(j\omega n) \mid n \in \mathbb{Z} \setminus \{0\}\}), \quad (14b)$$

$$\text{SRG}_{\underline{\mathcal{U}}_\omega}(G) = \text{co}_{\text{Be-KI}}(\{G(j\omega/n) \mid n \in \mathbb{Z} \setminus \{0\}\}), \quad (14c)$$

$$\text{SRG}(G) = \text{co}_{\text{Be-KI}}(\{G(j\tilde{\omega}) \mid \tilde{\omega} \in [0, \infty)\}), \quad (14d)$$

Our contribution is the SRG in Eqs. (14a), (14b) and (14c), whereas the SRG in Eq. (14d) was derived in [11].

2) *Computing nonlinear bode plots using SRGs:* An incrementally stable NL operator R preserves the input period, but can generate higher harmonics, therefore for a fixed $\omega \in \mathbb{R}_{>0}$

$$R : \underline{\mathcal{U}}_\omega \rightarrow \overline{\mathcal{U}}_\omega, \quad R : \overline{\mathcal{U}}_\omega \rightarrow \overline{\mathcal{U}}_\omega, \quad R : \underline{\mathcal{U}}_\omega \rightarrow L_{2e}. \quad (15)$$

Eq. (14) and (15) can be used to determine which input specific SRGs to use for the LTI parts of the LFR in Eq. (13) in the following way. First, define the SRG bound for an LFR of the form in Eq. (13) as

$$\begin{aligned} & \text{SRG}_{\mathcal{U}_1}(P_{ew}^S) (\text{SRG}(\phi)^{-1} - \text{SRG}_{\mathcal{U}_1}(P_{zw}^S))^{-1} \\ & \times \text{SRG}_{\mathcal{U}_2}(P_{zr}^S) + \text{SRG}_{\mathcal{U}_2}(P_{er}^S) =: \mathcal{G}_{\mathcal{U}_1, \mathcal{U}_2}^{\text{LFR}}(S), \end{aligned} \quad (16)$$

where $\mathcal{U}_1, \mathcal{U}_2$ are arbitrary sets. Note that Eq. (16) is evaluated using Proposition 1. Then, we can bound the SRG of S for specific input spaces as

$$\text{SRG}_{\underline{\mathcal{U}}_\omega}(S) \subset \mathcal{G}_{\underline{\mathcal{U}}_\omega, \underline{\mathcal{U}}_\omega}^{\text{LFR}}(S), \quad (17a)$$

$$\text{SRG}_{\overline{\mathcal{U}}_\omega}(S) \subset \mathcal{G}_{\overline{\mathcal{U}}_\omega, \overline{\mathcal{U}}_\omega}^{\text{LFR}}(S), \quad (17b)$$

$$\text{SRG}_{\underline{\mathcal{U}}_\omega}(S) \subset \mathcal{G}_{L_{2e}, \underline{\mathcal{U}}_\omega}^{\text{LFR}}(S), \quad (17c)$$

$$\text{SRG}(S) \subset \mathcal{G}_{L_{2e}, L_{2e}}^{\text{LFR}}(S). \quad (17d)$$

The sets in Eq. (17) relate to the frequency-dependent gains in Eq. (9) as

$$\Gamma_\omega(S) \leq r_{\min}(\mathcal{G}_{\mathcal{U}_\omega, \mathcal{U}_\omega}^{\text{LFR}}(S)) =: \hat{\Gamma}_\omega(S), \quad (18a)$$

$$\bar{\Gamma}_\omega(R) \leq r_{\min}(\mathcal{G}_{\mathcal{U}_\omega, \bar{\mathcal{U}}_\omega}^{\text{LFR}}(S)) =: \hat{\bar{\Gamma}}_\omega(S), \quad (18b)$$

$$\underline{\Gamma}_\omega(S) \leq r_{\min}(\mathcal{G}_{L_{2e}, \mathcal{U}_\omega}^{\text{LFR}}(S)) =: \hat{\underline{\Gamma}}_\omega(S), \quad (18c)$$

$$\Gamma(S) \leq r_{\min}(\mathcal{G}_{L_{2e}, L_{2e}}^{\text{LFR}}(S)) =: \hat{\Gamma}(S), \quad (18d)$$

where the hats are used to indicate that they are *upper bounds*, and not necessarily exact. By the same argument using which Eq. (10) was derived, we can conclude

$$\hat{\Gamma}_\omega(S) \leq \hat{\bar{\Gamma}}_\omega(S) \leq \hat{\Gamma}(S), \quad \hat{\Gamma}_\omega(S) \leq \hat{\underline{\Gamma}}_\omega(S) \leq \hat{\Gamma}(S). \quad (19)$$

Note that since $\lim_{\omega \rightarrow \infty} \mathcal{U}_\omega = \lim_{\omega \downarrow 0} \bar{\mathcal{U}}_\omega = L_{2e}$, we can conclude (analogous to Eq. (11)) that

$$\lim_{\omega \rightarrow \infty} \hat{\Gamma}_\omega(S) = \lim_{\omega \downarrow 0} \hat{\bar{\Gamma}}_\omega(S) = \hat{\Gamma}(S). \quad (20)$$

We denote $\hat{\omega}_B$ and $\hat{\omega}_c$ as the bandwidths that are estimated using Eq. (18) in Definitions 3 and 4. From Eq. (18) it is readily derived that

$$\hat{\omega}_B \leq \omega_B, \quad \hat{\omega}_c \geq \omega_c.$$

To summarize, one should follow the following recipe to compute the NL Bode plot.

- 1) Write the system S in LFR form to arrive at Eq. (13).
- 2) Compute the SRGs in Eq. (17) using Proposition 1.
- 3) Compute the radius to arrive at Eq. (18) and plot these values as function of frequency.

The analysis of the loop transfer L (or any other transfer) follows exactly the same analysis.

3) *Plants with integrators*: As mentioned in Section IV-A, we assume that $P_{yw}^L, P_{ze}^L, P_{ye}^L, P_{ew}^S, P_{zr}^S, P_{er}^S$ are stable and that $(\phi^{-1} - P_{zw}^L)^{-1}$ and $(\phi^{-1} - P_{zw}^S)^{-1}$ are incrementally stable on L_{2e} . However, when any of these LTI operators contains an integrator, which is commonplace in practice, the assumptions for our analysis would not hold.

However, noting that $\text{SRG}_{\bar{\mathcal{U}}_\omega}(G)$ is bounded for all G with only stable poles and integrators, we can still compute $\hat{\Gamma}_\omega(S)$ and $\hat{\bar{\Gamma}}_\omega(S)$ for all ω such that these bounds return a finite value. This can be understood from the LTI case, where an integrator is not Bounded-Input-Bounded-Output (BIBO) stable for all possible inputs, but is BIBO stable for periodic inputs.

This “extension” for plants with integrators is particularly useful for analyzing the loop transfer L , which commonly contains integrators. Examples of these cases are motion control setups [5].

D. Loop shaping

The frequency-dependent gain bounds in Eq. (18) can be used for the design of controllers with performance guarantees. We distinguish two different approaches: loop shaping and mixed-sensitivity shaping.

1) *Interpretation of the gain bounds*: In the NL case, one must use $\hat{\underline{\Gamma}}_\omega(S)$ to study the low-frequency behavior and $\hat{\bar{\Gamma}}_\omega(S)$ for the high-frequency behavior. The harmonic gain bound can also be used to provide a non-approximative upper bound for the frequency domain analysis methods in [8]. By studying $\hat{\bar{\Gamma}}_\omega(S)$, one addresses the question “what is the lowest frequency in the input for which the controller has no influence (i.e. $|S| \approx 1$)?” Conversely, by studying $\hat{\underline{\Gamma}}_\omega(S)$, one addresses the question “what is the highest frequency that can be allowed in the input to guarantee good tracking behavior?” Finally, one can use $\hat{\Gamma}_\omega(S)$ if one is interested in sinusoidal inputs specifically, for example in [5], [7].

2) *Application to loop shaping*: In the loop shaping case, one uses $\hat{\bar{\Gamma}}_\omega(L)$ to tune the open-loop bandwidth to a desired level. At the same time, $\hat{\Gamma}(S)$ provides an upper bound for the *modulus margin* and guarantees stability when $\hat{\Gamma}(S)$ is finite. The interpretation of performance in this NL loop shaping framework is the following: if the bandwidth is at most $\hat{\omega}_c$, then it is sure that the feedback loop is not sensitive to inputs with period $T = 2\pi/\hat{\omega}_c$ and higher harmonics.

Perhaps the more promising approach is mixed-sensitivity shaping. In that case, one computes Eq. (18) for any desired loop transfer T and tunes the controller to achieve the desired shape. Alternatively, one designs input and output LTI weighting filters W_{in} and W_{out} , respectively, for the relevant loop transfer, e.g. sensitivity S . Then, one attaches these to the LFR in Eq. (13), changing the LTI blocks in the LFR as $P_{ew}^S \rightarrow W_{\text{out}} P_{ew}^S, P_{zr}^S \rightarrow P_{zr}^S W_{\text{in}}$ and $P_{er}^S \rightarrow W_{\text{out}} P_{er}^S W_{\text{in}}$. The interpretation of performance in this NL mixed-sensitivity shaping framework is the following: if $\|r\|_{\text{RMS}} \leq 1$, then $\|e\|_{\text{RMS}} \leq 1$. This result can be seen as a NL generalization of the \mathcal{H}_∞ performance concept. If $\hat{\Gamma}(W_{\text{out}} S W_{\text{in}}) \leq 1$, we are guaranteed that for each frequency, a sinusoidal input with $\|r\|_{\text{RMS}} = \sqrt{|\hat{r}_1|^2 + |\hat{r}_{-1}|^2} \leq 1$ results in an output that satisfies $\|e\|_{\text{RMS}} \leq 1$, which implies $\sqrt{|\hat{e}_1|^2 + |\hat{e}_{-1}|^2} \leq 1$, and satisfies the performance specifications encoded in the weighting filters.

E. Comparison with Existing Methods

There are several existing methods to study the frequency-dependent gain of NL systems. The oldest and most well-known is the *describing function method* (DF) [4]–[6]. This method is only approximate and considers only the first harmonic in the response to a sinusoidal input. The advantage is that the gain can be computed for different input amplitudes and considers phase. The DF has been extended to include all harmonics in the output [7], [13] and even to consider inputs that contain harmonics [8], [9].

The main advantage of our result (18) is that it is not approximate, compared to the DF method. The sinusoidal gain $\hat{\Gamma}_\omega(R)$ can be used to reproduce the DF methods that consider sinusoidal input. However, $\hat{\Gamma}_\omega(R)$ considers all magnitudes of the input. To obtain input amplitude-dependent results, one should constrain $\text{SRG}_{\mathcal{U}}(\phi)$ to an input space \mathcal{U} of certain amplitude.

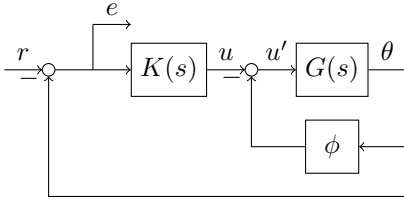


Fig. 3: Block diagram of the controlled DC motor in the example.

Whereas $\hat{\Gamma}_\omega(R)$ and $\hat{\Gamma}_\omega(R)$ can be compared with existing methods, we must emphasize that there exists no method that considers *subharmonic* inputs, to the best of our knowledge. Therefore, the subharmonic gain $\hat{\Gamma}_\omega(R)$ provides a novel way to analyze the frequency domain behavior of the system, especially in the low-frequency regime.

V. EXAMPLE

A. The Controlled Nonlinear DC Motor

As an example, we will consider the position control of a DC motor. The equations of motion follow from Newton's second law and Kirchhoff's law with back emf

$$J\ddot{\theta} + b\dot{\theta} = K_m i, \quad (21)$$

$$L \frac{di}{dt} + Ri + \delta \sin(\theta) = u - K_m \dot{\theta}, \quad (22)$$

where θ (rad) is the angular position of the rotor, u (V) is the input voltage and i (A) is the resulting current in the armature of the the motor. Furthermore, the parameters in Eqs. (21) and (22) are $J = 0.1 \text{ kg m}^2$, $R = 0.96 \Omega$, $L = 1 \text{ H}$, $K_m = 0.2$, $b = 1.0044 \text{ N m s}$, while $\delta = 0.1$ is the magnitude of a parasitic NL effect in the motor. By substituting Eq. (21) into Eq. (22), neglecting the NL term $\delta \sin(\theta)$, one obtains the transfer function $\theta = Gu$ given by

$$G(s) = \frac{1}{s} \frac{Js + b}{(Ls + R)(Js + b) + K_m^2}, \quad (23)$$

where $s \in \mathbb{C}$ is the Laplace variable. For the control configuration, we consider a standard setpoint control problem with reference r (rad) and tracking error $e = r - \theta$. Let $u = Ke$ be the controller composed of a a gain and lead filter

$$K(s) = 5 \frac{s + 1}{s/10 + 1}, \quad (24)$$

for which the LTI sensitivity $S_{\text{LTI}} = 1/(1 + GK)$ is stable.

To take the nonlinearity in Eq. (22) into account, we define $u' = u - \phi(\theta) = u - \delta \sin(\theta)$. The resulting feedback interconnection for the controlled NL DC motor is depicted in Fig. 3.

B. Frequency Domain Analysis of the Nonlinear Model

To study the NL model in the frequency domain, we evaluate the right hand side of Eq. (18) for both the loop transfer $L : e \mapsto \theta$ and the sensitivity $S : r \mapsto e$.

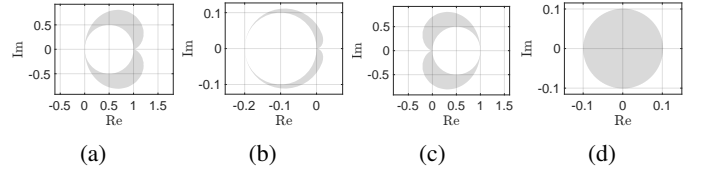


Fig. 4: SRGs for computing $\hat{\Gamma}(S)$. (a) $\text{SRG}(P_{er}^S)$, (b) $\text{SRG}(P_{zw}^S)$, (c) $\text{SRG}(P_{zr}^S)$, (d) $(\text{SRG}(\phi)^{-1} - \text{SRG}(P_{zw}^S))^{-1}$.

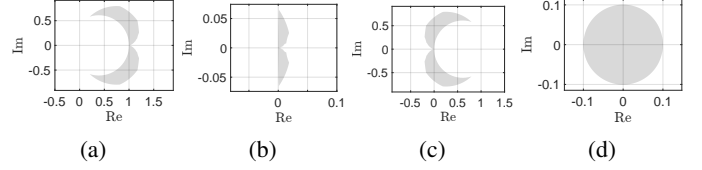


Fig. 5: SRGs for computing $\hat{\Gamma}_3(S)$. (a) $\text{SRG}_{\bar{U}_3}(P_{er}^S)$, (b) $\text{SRG}_{\bar{U}_3}(P_{zw}^S)$, (c) $\text{SRG}_{\bar{U}_3}(P_{zr}^S)$, (d) $(\text{SRG}(\phi)^{-1} - \text{SRG}_{\bar{U}_3}(P_{zw}^S))^{-1}$.

1) *SRG computation:* The first step is to write these operators in the LFR form of (12) and (13). By setting $w = \phi(z)$, we obtain after some simple calculations that

$$\begin{aligned} P_{zw}^L &= -G, P_{\theta w}^L = -G, P_{ze}^L = L_{\text{LTI}}, P_{\theta e}^L = L_{\text{LTI}}, \\ P_{zw}^S &= -S_{\text{LTI}}G, P_{ew}^S = S_{\text{LTI}}G, P_{zr}^S = S_{\text{LTI}}GK, P_{er}^S = S_{\text{LTI}}. \end{aligned}$$

Second, we need to compute the SRGs of the nonlinearity. From [11] we know that $\text{SRG}(\phi) \subset D_{[-\delta, \delta]}$.

To illustrate how Eq. (18) is evaluated, we show the SRG computations explicitly for some frequency values. In Fig. 4, the necessary SRGs are plotted to evaluate Eq. (16) to compute $\hat{\Gamma}(S)$. Because all sets that are multiplied in Eq. (16) using Proposition 1.d. have finite radius, the resulting bound $\hat{\Gamma}(S)$ must be bounded. Similarly, in Figs. 5 and 6 we show the SRGs that are required to compute $\hat{\Gamma}_3(S)$ and $\hat{\Gamma}_1(L)$, respectively, and these yield bounded results. To illustrate the problem that might occur with integrators, as discussed in Section IV-C3, we compute the necessary SRGs for $\hat{\Gamma}_{0.05}(L)$ in Fig. 7. Because $\text{SRG}(\phi)^{-1}$ and $\text{SRG}_{\bar{U}_{0.05}}(P_{zw}^L)$ overlap, it holds that $0 \in \text{SRG}(\phi)^{-1} - \text{SRG}_{\bar{U}_{0.05}}(P_{zw}^L)$, hence the SRG bound in Eq. (16) becomes unbounded.

In all cases, the SRG sums, products and inverses are computed using Proposition 1. Additionally, chord or arc segments are added to the SRGs if required for a sum or product operation, respectively.

2) *Sensitivity analysis:* The third and last step is to evaluate Eq. (18) on a grid of frequency points. The result for the sensitivity S is plotted in Fig. 8a where we also included S_{LTI} for comparison.

First of all, we can read off, using Eq. (20), that $\hat{\Gamma}(S) = 2.24 \text{ dB} = 1.29$, concluding $\Gamma(S) \leq 1.29$. Now in the LTI case, one uses S_{LTI} to study both the low- and high-frequency behavior. As explained in Section IV-D1, we use $\hat{\Gamma}_\omega(S)$ and $\hat{\Gamma}_\omega(S)$ to study the low- and high-frequency behavior, respectively.

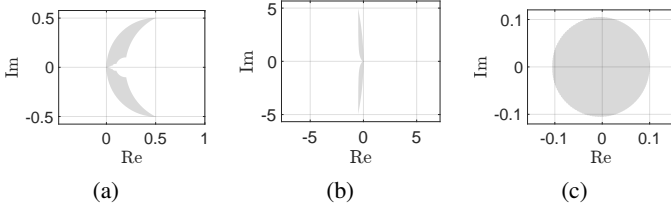


Fig. 6: SRGs for computing $\hat{\Gamma}_1(L)$. (a) $\text{SRG}_{\bar{U}_1}(P_{zw}^L)$, (b) $\text{SRG}_{\bar{U}_1}(P_{ze}^L)$, (c) $(\text{SRG}(\phi)^{-1} - \text{SRG}_{\bar{U}_1}(P_{zw}^L))^{-1}$.

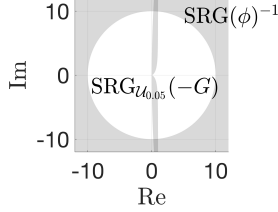


Fig. 7: $\text{SRG}(\phi)^{-1}$ and $\text{SRG}_{\bar{U}_{0.05}}(P_{zw}^L)$

From $\hat{\Gamma}_\omega(S)$ in Fig. 8a we can read off what the highest frequency is that can be allowed in the input to achieve good tracking performance. As is clear from Fig. 8a, the NL Bode diagram provides this information and predicts a closed-loop bandwidth estimate of $\hat{\omega}_B = 3.3\text{rad}$. The harmonic gain bound can also be used to provide a non-approximative upper bound for the frequency domain analysis methods in [8].

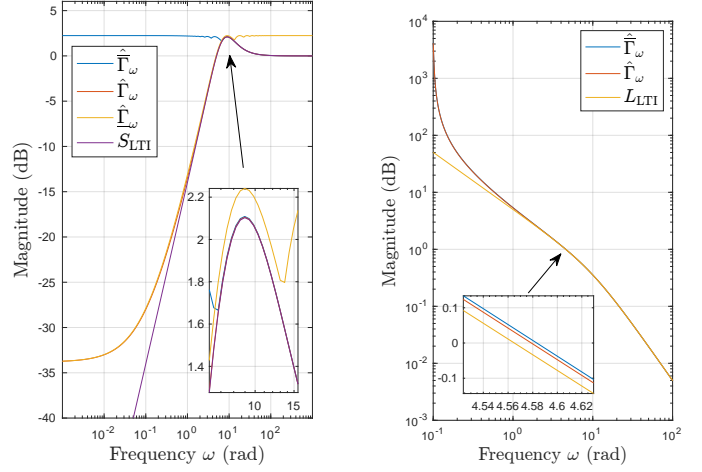
Conversely, from $\hat{\Gamma}_\omega(S)$ in Fig. 8a what the response of the system is to high frequency inputs, including harmonics. The NL Bode diagram gives a frequency region in which $\hat{\Gamma}_\omega(S)$ increases from 1 to $\hat{\Gamma}(S)$. However, for low-frequency behavior, $\hat{\Gamma}_\omega(S)$ is not useful.

From $\hat{\Gamma}_\omega(S)$ in Fig. 8a one can see what the response is to sinusoidal inputs, and resembles a typical LTI sensitivity graph. However, the harmonic and subharmonic gain bounds offer a far more general result.

One particularly interesting feature that is present in Fig. 8a is the fact that the integrator behavior in S_{LTI} is no longer present in the NL case. Overall, it seems that the low-frequency behavior differs more from the LTI case than the high-frequency behavior. We will verify these observations in Section V-C.

3) *Loop transfer analysis:* For the loop transfer L , we do not compute the subharmonic part from Eq. (18). The reason for this is that the LTI parts of the LFR for L contain an integrator. Therefore, as explained in Section IV-C3, the subharmonic gain will always be infinite. The relevant frequency-dependent incremental gain bounds for L are plotted in Fig. 8b, where L_{LTI} is included for comparison.

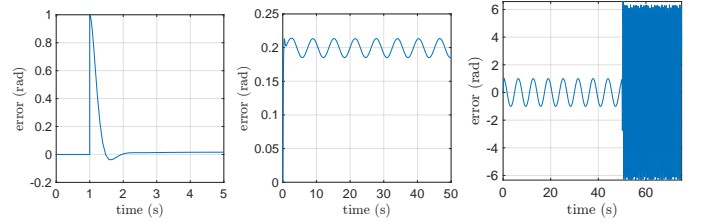
From $\hat{\Gamma}_\omega(L)$ in Fig. 8b we can read off that $\hat{\omega}_c = 4.58\text{rad}$. Furthermore, we see that both the sinusoidal gain $\hat{\Gamma}_\omega(L)$ and harmonic gain $\hat{\Gamma}_\omega(L)$ diverge at a finite nonzero value of ω . The reason for this is that $r_{\min}((\text{SRG}(\phi)^{-1} - \text{SRG}_{\mathcal{U}}(P_{zw}^L))^{-1})$ diverges due to the integrator in G , where $\mathcal{U} \in \{\mathcal{U}_\omega, \bar{\mathcal{U}}_\omega\}$.



(a) NL sensitivity bode diagram for the DC motor.

(b) NL loop transfer bode diagram for the DC motor.

Fig. 8: NL Bode diagrams for sensitivity and loop transfer.



(a) Step input r_1 , (b) Ramp input r_2 , (c) Periodic input r_3 . steady state error 0.0167.

Fig. 9: Simulated responses of the controlled NL DC motor.

4) *Nonlinear gain upper bounds the LTI Gain:* Note that since $P_{\theta e}^L = L_{\text{LTI}}$ and $P_{er}^S = S_{\text{LTI}}$ and both S_{LTI} and L_{LTI} converge to zero, we can add $|L_{\text{LTI}}(j\omega)| \leq \hat{\Gamma}_\omega(L)$ and $|S_{\text{LTI}}(j\omega)| \leq \hat{\Gamma}_\omega(S)$ to the inequalities in Eq. (19). From Figs. 8a and 8b one can see that these inequalities indeed hold.

An immediate consequence is that $\hat{\omega}_B \leq \omega_B^{\text{LTI}}$, $\hat{\omega}_c \geq \omega_c^{\text{LTI}}$, where ω_B^{LTI} and ω_c^{LTI} are the closed-loop and open-loop bandwidth, respectively. Note that in the LTI case, we do not need a hat to indicate the estimate since we can compute the bandwidths exactly using the LTI bode diagram.

C. Simulation Results

We simulate the system in Fig. 3 for three different references, a step r_1 , ramp r_2 , and periodic signal r_3 that switches between two different frequencies, defined by

$$r_1(t) = \begin{cases} 0 & \text{if } t \leq 1, \\ 1 & \text{else,} \end{cases} \quad r_2(t) = t, \quad r_3(t) = \begin{cases} 5 \sin(t) & \text{if } t \leq 50, \\ 5 \sin(10t) & \text{else.} \end{cases}$$

Using the step reference r_1 , one can see from Fig. 9a that the step response settles at a nonzero steady state error is $0.0167 = -35.5\text{dB}$. This corresponds to the observation that the gain $\hat{\Gamma}_\omega(S)$ in the NL Bode diagram Fig. 8a has no

integrator behavior. Moreover, we see that $\hat{\Gamma}_0(\omega) \approx -34\text{dB}$, which provides an upper bound for the steady state error, analogous to the LTI case.

The simulation of the ramp reference r_2 in Fig. 9b reveals a periodic response to a non-periodic input, which is a NL effect not present in the LTI model S_{LTI} . The period of the disturbance is 1rad/s , corresponding to the nonlinearity $\propto \sin(\theta)$, where θ tracks $r_2(t) = t$.

Finally, the simulation of the reference r_3 , which switches between two sinusoidal signals of different frequencies, reveals two things. First of all, one can read off that the amplitude gain is 1.01 for $\omega = 1\text{rad/s}$, while the amplitude gain for 10rad/s is 6.3. We see that $\hat{\Gamma}_1(S) \approx -13.45\text{dB} = 0.213$ and $\hat{\Gamma}_{10}(S) \approx 2.05\text{dB} = 1.27$. This corresponds to the input amplitude of 5, since $5 \cdot \hat{\Gamma}_1(S) \approx 1.06$ and $5 \cdot \hat{\Gamma}_{10}(S) \approx 6.3$, recovering the amplitude of e in the steady state regimes. Note that $\hat{\Gamma}_\omega(S)$ provides *upper bounds* for the amplitude, not merely approximations like the describing function. Secondly, it is clear that there is no large transient behavior at the transition points at $t = 0$ and $t = 50$, which warrants the use of the NL Bode diagram to describe the performance of the system.

VI. CONCLUSION

This paper develops graphical frequency domain analysis tools for incrementally NL stable systems. The NL Bode diagram goes beyond existing methods that are restricted to sinusoidal inputs. In addition, we can compute the gain for subharmonic input signals, enabling a precise low-frequency sensitivity analysis. We briefly highlight how our method can be used for NL loop shaping. Our results offer a clear interpretation in the frequency domain and a definition of the NL bandwidth. Finally, the effectiveness of our method is demonstrated on the position control of a NL DC motor.

REFERENCES

- [1] H. Nyquist, "Regeneration Theory," *Bell System Technical Journal*, vol. 11, no. 1, pp. 126–147, Jan. 1932.
- [2] H. W. Bode, "Relations Between Attenuation and Phase in Feedback Amplifier Design," *Bell System Technical Journal*, vol. 19, no. 3, pp. 421–454, Jul. 1940.
- [3] S. Skogestad and I. Postlethwaite, *Multivariable Feedback Control: Analysis and Design*, 2nd ed. Chichester: Wiley, 2010.
- [4] N. M. Krylov, N. N. Bogoliubov, and S. Lefschetz, *Introduction to Non-Linear Mechanics*, ser. Annals of Mathematics Studies; Annals of Mathematics Studies; No. 11; No. 11. Princeton: Princeton University Press, 1947.
- [5] A. Pogromsky and R. Van Den Berg, "Frequency Domain Performance Analysis of Lur'e Systems," *IEEE Transactions on Control Systems Technology*, vol. 22, no. 5, pp. 1949–1955, Sep. 2014.
- [6] M. F. Heertjes, "Variable Gain Motion Control of Wafer Scanners," *IEEE Journal of Industry Applications*, vol. 5, no. 2, pp. 90–100, 2016.
- [7] A. Pavlov, N. Van De Wouw, A. Pogromsky, M. Heertjes, and H. Nijmeijer, "Frequency domain performance analysis of nonlinearly controlled motion systems," in *2007 46th IEEE Conference on Decision and Control*. New Orleans, LA, USA: IEEE, 2007, pp. 1621–1627.
- [8] D. Rijlaarsdam, P. Nuij, J. Schoukens, and M. Steinbuch, "A comparative overview of frequency domain methods for nonlinear systems," *Mechatronics*, vol. 42, pp. 11–24, Apr. 2017.
- [9] A. Pavlov, B. Hunnekens, N. Wouw, and H. Nijmeijer, "Steady-state performance optimization for nonlinear control systems of Lur'e type," *Automatica*, vol. 49, no. 7, pp. 2087–2097, Jul. 2013.

- [10] E. K. Ryu, R. Hannah, and W. Yin, "Scaled relative graphs: Nonexpansive operators via 2D Euclidean geometry," *Mathematical Programming*, vol. 194, no. 1-2, pp. 569–619, Jul. 2022.
- [11] T. Chaffey, F. Forni, and R. Sepulchre, "Graphical Nonlinear System Analysis," *IEEE Transactions on Automatic Control*, vol. 68, no. 10, pp. 6067–6081, Oct. 2023.
- [12] J. P. J. Krebbeckx, R. Tóth, and A. Das, "SRG Analysis of Lur'e Systems and the Generalized Circle Criterion," Nov. 2024, accepted for ECC 2025.
- [13] A. Pavlov, N. van de Wouw, and H. Nijmeijer, Eds., *Uniform Output Regulation of Nonlinear Systems: A Convergent Dynamics Approach*, ser. Systems and Control: Foundations & Applications. Boston, MA: Birkhäuser Boston, 2006.
- [14] C. A. Desoer and M. Vidyasagar, *Feedback Systems: Input-Output Properties*, ser. Electrical Science Series. New York: Acad. Press, 1975.
- [15] A. Van Der Schaft, *L2-Gain and Passivity Techniques in Nonlinear Control*, ser. Communications and Control Engineering. Cham: Springer International Publishing, 2017.
- [16] K. Zhou, J. C. Doyle, K. Glover, and J. C. Doyle, *Robust and Optimal Control*. Upper Saddle River, NJ: Prentice Hall, 1996.